

# A detailed model deduction and parameter values for the Tennessee-Eastman benchmark

Mateo Arcila-Osorio<sup>1,2\*</sup>, Carlos Ocampo-Martinez<sup>1,2†</sup> and  
Hernan Alvarez<sup>3†</sup>

<sup>1\*</sup> Automatic Control Department, Universitat Politècnica de Catalunya  
- BarcelonaTech, 08028 Barcelona, Spain.

<sup>2\*</sup> Institut de Robòtica i Informàtica Industrial, CSIC-UPC, 08028  
Barcelona, Spain.

<sup>3</sup> Process and Energy Department, Universidad Nacional de Colombia,  
050034 Medellín, Colombia.

\*Corresponding author(s). E-mail(s): [mateo.arcila@upc.edu](mailto:mateo.arcila@upc.edu);  
Contributing authors: [carlos.ocampo@upc.edu](mailto:carlos.ocampo@upc.edu); [hdalvare@unal.edu.co](mailto:hdalvare@unal.edu.co);

†These authors contributed equally to this work.

## Abstract

This paper presents a detailed deduction of the model introduced in the recognized Tennessee-Eastman (TE) benchmark process. The purpose is to show the majority of process operation considerations and the not so obvious assumptions applied by Downs and Vogel during the model statement in their seminal paper. This objective is achieved by providing the details of the deduction of a phenomenological-based semi-physical model (PBSM) for the TE plant. This implemented modelling approach is completely described whereas the equations are derived individually for each relevant piece of equipment (reactor, condenser-flash separator, stripping tower, and mixing point). Then, such equations are integrated to construct the final model of the plant. It was feasible to simulate the four fundamental modes of plant operation, achieving alignment with the steady-state values documented in prior research. Furthermore, the values of additional parameters that were not previously available in the literature were determined, providing other researchers with the opportunity to readily simulate those operation modes of the plant. Finally, some relevant simulation results are presented, including the system responses to disturbances, along with a discussion about determining the process initial conditions.

**Keywords:** Benchmark, industrial chemical process, parameters values, phenomenological-based semi-physical model, plant-wide system, Tennessee-Eastman

## 1 Introduction

For many years, researchers in the control field have been interested in formulating real problems in industrial processes to test several control strategies through simulations. In 1993, [Downs and Vogel \(1993\)](#), from the control group of the corporate processes at Eastman Chemical Company, introduced a real process suitable as a reference problem (benchmark). This work, widely known as the Tennessee-Eastman (TE) process, was consolidated some time later in other studies. Downs and Vogel modified the components, the reaction kinetics, the process diagram, and the operating conditions of the real problem, all for patent protection. However, this problem is based on a real industrial process, not an artificial one. The details were documented in an article that includes a process description, the control objectives, and information on streams and their respective steady-state molar fractions and flow rates for the base case of plant operation. The original process model was encoded into a set of FORTRAN subroutines describing non-linear relationships from the material and energy balances. Although the authors did not share the equations of this model in the original document, they indicated that to obtain this data at that time, interested people should send an email request, after which the information would be sent via a floppy disk.

The TE process has served as a worldwide reference problem for the design of suitable control strategies to be applied in such process plants. In 1995, [Ricker and Lee \(1995b\)](#) introduced the equations of a non-linear, mechanistic model of the TE process and provided applications for its use in on-line monitoring and control tasks, as well as for state estimation. In contrast to the original work, Ricker and Lee presented explicit model equations describing thermodynamic relationships for each unit operation in the plant and their corresponding material balances. They cited their own previous work ([Ricker, 1993](#)) on the TE process, suggesting that Downs and Vogel were not the only ones to address this problem in the past. Although the authors present the model equations, they do not provide their derivation or justify the underlying assumptions, either in that work or in any subsequent publications. Certainly, a detailed deduction of the model equations contributes to assimilate the process phenomenology, which has not been published until now. In other work, [Ricker and Lee \(1995a\)](#) presented the development and evaluation of a non-linear model predictive control (NMPC) strategy applied to the challenging TE process, showcasing one of the first applications of this benchmark. Besides, many other authors have also worked on this application ([Elorza Casas et al., 2023](#); [Tătulea-Codrean et al., 2020](#); [Ravi Srinivas and Arkun, 1997](#); [Zhou and Zhu, 2022](#); [Jämsä, 2018](#)).

In 2002, the application and evaluation of different multivariate statistical process monitoring methods, such as moving principal component analysis (MPCA) for detecting abnormalities in the TE process was discussed, constituting one of the

pioneer statistical applications on this benchmark (Kano et al., 2002). In 2003, the OptControlCentre tool was used for the dynamic optimization of the TE process. This tool is a platform designed for optimizing and implementing advanced control in industrial processes. The approach aims to identify the best operating conditions over time to enhance production, energy efficiency, and product quality. This work by Jockenhövel et al. (2003) explains the models used, adjustments, and optimization algorithms. Moreover, equations representing material and energy balances are reported. Another study demonstrating the effectiveness of this proposed approach in enhancing performance under various operating conditions was presented by Tian and Hoo (2003).

On the other hand, Bathelt et al. (2015) developed a modified version of the TE process model that addresses inconsistencies in simulation results caused by changes in MATLAB simulation software. These authors highlight reproducibility challenges associated with different numerical solvers. Likewise, it can be seen that the Euler method is relatively stable and performs reliably for simulation purposes. Key improvements include ensuring independent simulation results that remain consistent regardless of the solver or simulation time increment, and enhancing efficiency through reducing simulation time by approximately 45% compared to the original model. The modified model also incorporates extended process measurements and disturbances, along with new monitoring outputs. Likewise, Martin-Villalba et al. (2018) presented two Modelica libraries designed for modelling the TE process. The authors emphasize the absence of object-oriented implementations of such a process in modelling languages like Modelica, despite numerous existing simulators in other languages. Both libraries have been validated against literature data, demonstrating their potential for reuse in advanced process control and optimization studies. In 2022, pyTEP was introduced as an open-source Python application programming interface (API) for the TE process, enabling more flexible and user-friendly simulation beyond traditional fault detection applications (Reinartz and Enevoldsen, 2022). Besides, Vosloo et al. (2025) present a comprehensive TE simulator developed in Simulink.

All the previous works, along with many more existing in the literature, except the cited (Ricker and Lee, 1995b) and (Jockenhövel et al., 2003) papers, present applications, simulation results, and improvements of the existing simulators, but often lack a detailed description that clearly outlines the structure of the model. Many of them primarily focus on achieving results from the seminal article, illustrating implemented control strategies without delving into the details of assumptions, equipment analysis, and the equations used. Sometimes a dichotomy is observed in the equations, some are presented in their entirety, whereas others are simplified, leaving crucial details unaddressed for simulating the plant accurately. With a complete derivation of the model and its assumptions, the benchmark could be applied beyond control or estimation tasks to other areas of process engineering, such as modeling, design, and teaching, as suggested by Udugama et al. (2020).

Recent applications of the TE benchmark have extensively employed machine learning (ML), data analytics, and artificial intelligence (AI) techniques to enhance process monitoring and fault detection. The works have used deep learning models for unsupervised anomaly detection, demonstrating improved fault diagnosis capabilities

in complex chemical processes (Hartung et al., 2023). Additionally, deep neural network architectures have been tested for their effectiveness in fault detection within the TE process, highlighting the potential of AI-driven approaches (Chadha and Schwung, 2017). However, whereas these data-driven models offer significant advantages, they often operate as black boxes, lacking transparency in their decision-making processes. In contrast, models based on first-principles, grounded in the fundamental physical and chemical laws governing the process, provide clear interpretability and insight into system behaviour.

Since the original equations from (Downs and Vogel, 1993) article were only available by mail request in 1993 and are not shared online, a thorough deduction of the TE model is valuable. This fact ensures a better understanding of the problem and a complete interpretation of the process behaviour. Furthermore, the aforementioned works would have been greatly enhanced with a detailed deduction of the model. Despite many control strategies applied to the TE benchmark are not based on explicit or highly accurate process models, the lack of a rigorously derived, unified model remains a significant limitation, particularly for new users of the benchmark. The availability of a detailed derivation of the model equations and a clear explanation of the validity of the model assumptions give the user high confidence in the ability of the model as a representation of a real process. Consequently, the current work concentrates on reengineering the seminal article, drawing support from other relevant studies, to obtain more comprehensive information and thereby showing the deduction of a phenomenological-based semi-physical model (PBSM) for the TE process. Moreover, since this work aims to reproduce the steady-state values of the four fundamental operation modes (base case (Downs and Vogel, 1993) and mode 1, 2, and 3 (Ricker and Lee, 1995b)), it is important to recall that, at each operation mode, the values of all variables and parameters must remain constant over time.

The PBSM approach produces mathematical models that are a combination of both white-box and black-box models (Alvarez, 2024). The basic structure of the model is completely derived from first-principles. However, the proposed model also includes some parameters that can be adjusted based on experimental data (Lema-Perez et al., 2019). In summary, the methodology steps include describing the process, defining a precise modelling objective, identifying the relevant process systems (PSs), and building the basic structure of the model. This step is accomplished by applying material, momentum, and energy balances on the defined PSs. Following these steps, additional constitutive and assessment equations are incorporated into the model, constituting the extended structure of the model, which enables the evaluation of both structural and functional parameters. Then, a computational routine is developed to solve the model equations simultaneously. Additionally, available experimental data are subsequently compared with the model outputs under specific operating conditions to validate the deduced model. Finally, model reproducibility is a key concern in the modelling and simulation community, as it ensures that results can be verified and compared across studies. Hence, we include direct comparisons that show the reproducibility of our model outputs.

The models that are obtained by rigorously following this modelling methodology have relevant properties such as generalization capacity, modularity, and interpretability of parameters. This methodology consist of 10 defined steps and has been used in other works for proposing process models (Alvarez and Ocampo-Martinez, 2022; Lema-Perez et al., 2019; Arbeláez-Gómez et al., 2022; Alvarez et al., 2009). The 10 steps of the methodology can be divided into three main sections: model pre-construction, model construction, and model validation. These sections are used in the sequel to deduce a PBSM for the TE process, but without including energy balances, contrary to what Jockenhövel et al. (2003) stated. Thus, the objective of Downs and Vogel’s seminal paper is not altered. The subsequent subsections are explained in great detail for the development of the reactor model. Although this methodology is applied identically to deduce the models of the other process equipment, only the essential is presented here to avoid an excessive extension of the manuscript. However, the reader is encouraged to access the comprehensive deduction of such models in the supplementary material of this paper.

The main contribution of this work is to provide the reader with a detailed model, initial conditions, and a set of parameters values to simulate the four main operation modes of the well-known TE process, given that complete data was only available for the base case of plant operation. The other three operation modes did not have published values for all parameters and initial conditions. Likewise, a systematic approach to obtain such information is presented. Besides, the development of the model includes a discussion about the main assumptions and considerations of the original benchmark and subsequent works. That discussion acts as a foundation of the model, providing increased credibility and reality.

This paper is organized as follows: Section 2 provides the model pre-construction, including a brief description of the plant and the process flow diagram (PFD). Section 3 describes the model construction, including the model equations. Section 4 presents the model validation with some relevant results. The calculation of the initial conditions and the parameters values are shown in Section 5. Finally, the conclusions of the work are drawn in Section 6.

## 2 Model pre-construction

In this section, the set of the first three steps of the PBSM methodology, called model pre-construction, is applied to the TE process. These three steps include the process description and model objective, the modelling hypothesis and level of detail, and the PSs definition. The plant as a whole is described in brief in the following, before developing the model pre-construction for each piece of equipment forming the plant. Other perspectives and descriptions are left to the readers, depending on their specific intentions for using the benchmark.

The TE process has a set of equipment used in a wide range of industrial chemical plants. The PFD of the plant is illustrated in Fig. 1, adding new stream numbers (14 to 19) with respect to the PFD given in the original paper by Downs and Vogel (1993). Some streams are internal and were defined only to facilitate the modelling task; they

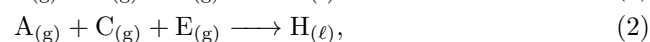
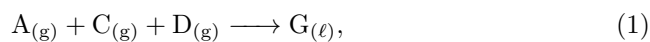
will be detailed in later sections. The plant consists of a reactor, a condenser, a liquid-vapour separator, a recycle compressor and a stripping column. A mixing point is required before the reactor in order to guarantee the homogenization of the several streams forming the reactor feed. The reactor is a continuous stirred tank reactor (CSTR) that operates with two phases, generating products G and H from reactants A, C, D, and E. An inert species B and a byproduct F, originated from two other undesired reactions, also participate. All reactions are exothermic and irreversible and occur simultaneously (in parallel). The effluent leaves the reactor through stream 7 as a mixture of gases and vapours. It then proceeds to the condenser, where the vapours transition into the liquid phase, facilitated by water as the cooling medium, while the gaseous compounds remain in the gas phase. This stream gets into the liquid-vapour separator or flash tank, where gas and liquid streams are produced. Part of the gas that leaves through stream 17 is purged through stream 9 to avoid accumulations of inert B and byproduct F. The remaining material in stream 17 undergoes compression to contribute to the recycle into the reactor. The liquid exiting the liquid-vapour flash separator through stream 10 carries the plant target products. However, such a liquid is contaminated with traces of other compounds that were not entirely separated in the flash tank. For this reason, the mentioned effluent is directed to a stripping tower. In this tower, a vapourizer is employed to introduce heat into the process, thereby maintaining thermal equilibrium between the phases. Thus, in the stripper, the products of interest (G and H) are obtained in the bottom stream 11. This separation is achieved through mass transfer with stream 4, which is a gas phase containing mainly A and C, but with traces of B. On the other hand, the head stream 5 of this stripping tower contains all the compounds involved in the process. This stream joins other streams to form the complete recycle. Finally, this mixture is combined at the mixing point with the fresh reagents that are fed into the reactor.

## 2.1 Reactor submodel pre-construction

The term *submodel* is used here and in the following to express that these specific models of pieces of equipment will comprise the final model of the TE process.

### 2.1.1 Process description and modelling objective

The CSTR plays a fundamental role in the process, serving as the heart of the plant. It is the equipment where the necessary reactions are carried out to obtain the desired compounds. The reactor is equipped with a cooling mechanism. As mentioned before, the objective is to produce the compounds of interest, G and H, through two main reactions, although there are two other undesired reactions that produce compound F. The original work by [Downs and Vogel \(1993\)](#) reported four reactions, but for the last one no kinetic data were found in the literature. However, this reaction can be integrated into the other three, yielding



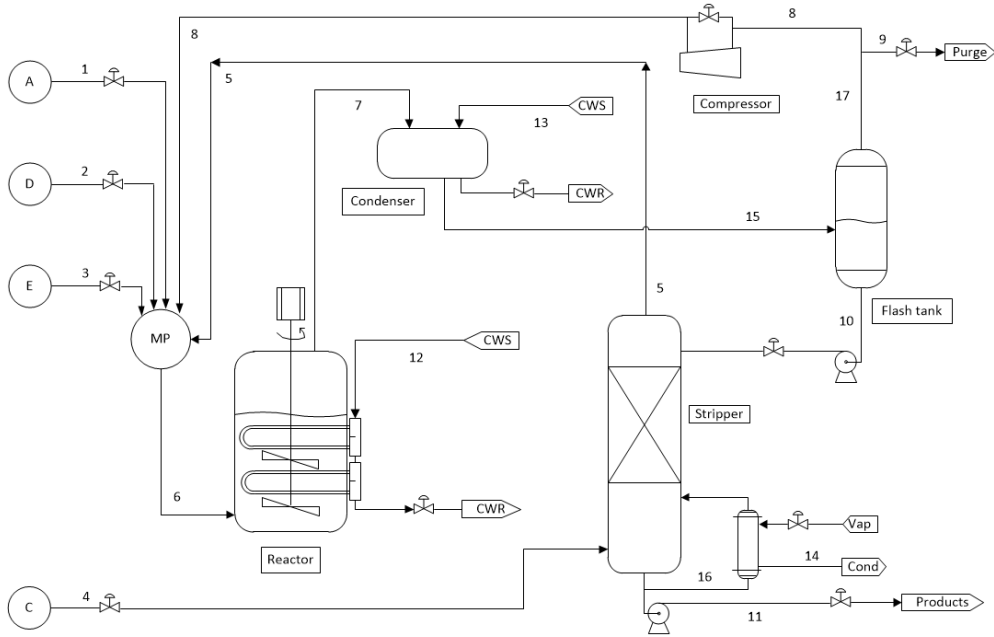
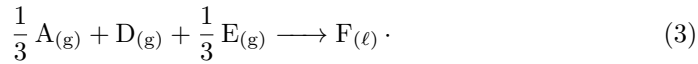


**Fig. 1** Process flow diagram (PFD) of the TE plant, adapted from the original by adding missing stream numbers.



**Remark 1.** The three reactions presented by [Ricker and Lee \(1995b\)](#), integrating the originals, are used here, clarifying that the last equation perfectly summarizes reactions 3 and 4 of the original paper.

All of the reactions are exothermic, irreversible, and exhibit a reaction rate dependent on the operating temperature of the reactor, the partial pressure of the gaseous fed reactants, and the volume of the reactor. It is worth noting that all products are in liquid form (indicated by the subscript  $\ell$ ), while all reactants are in gaseous state (indicated by the subscript  $g$ ). Additionally, an inert compound B enters and exits the reactor as a gas. The heat from the reactions is removed by internal heat exchangers that use cooling water (stream 12) as the thermal fluid. It is important to note that both liquid and gas phases are involved in the reactor, and this implies a particular operation of this equipment. Stream 6, which contains all reactants, inert B, and traces of both desired and undesired products, is introduced into the reactor. After participating in the chemical reactions, the resulting products, unreacted reactants, and inert B exit the reactor as gases and vapours through stream 7. Finally, the modelling objective consist of predicting the changes on the moles into the reactor for each one of the chemical species involved in this equipment.

### 2.1.2 Modelling hypothesis and level of detail

The modelling hypothesis to be used assumes that a gas chamber containing traces of vapours from condensable substances forms at the top of the reactor. It is within this gas-vapour space that chemical reactions take place, whose products, all liquids, pass into the liquid phase of the reactor. These reactions are catalyzed by a non-vapourizing liquid substance that remains within the reactor. A notable aspect is that there is no purge of the liquid phase from the reactor. However, in real operation, periodic purging of the liquid phase is necessary to prevent the accumulation of unwanted substances in the stagnant liquid inside the reactor. Additionally, to avoid losing the liquid catalyst during purging, a method must be ensured to retain the catalyst within the reactor. Considering the model objective, such a model will be addressed with a macroscopic level of detail and with the following main assumptions:

- A1. Components A, B, and C are insoluble in the liquid phase (see Remark 2).
- A2. The ideal gas equation of state applies to all gases and vapours.
- A3. All phases are well mixed.
- A4. The vapour-liquid equilibrium follows a modified Raoult's law.
- A5. Thermal and chemical liquid-vapour equilibrium inside the reactor is instantaneous.
- A6. The reactor is perfectly stirred and the energetic effects of the stirrer are negligible.

**Remark 2.** *While assumption A1 holds perfectly for the reactor and the flash separator, it is worth noting that in the stripping tower, traces of compounds A, B, and C are present in the outlet liquid stream.*

### 2.1.3 Process Systems (PSs) definition

A PS is an arbitrary abstraction of a part of the process to which all the tools available in systems theory can be applied. A key factor in determining PSs is to identify physical separations or barriers within the process, as well as distinguishable phase changes or characteristics of the mass that indicate spatial differences (Hangos and Cameron, 2001). Taking into account the level of detail defined for the model, four PSs will be taken, as shown in Fig. 2. The four PSs considered are as follows: PS I, corresponding to the gas-vapour contained in the upper part of the reactor; PS II, representing the liquid phase inside the reactor without considering the volume of the liquid catalyst; PS III, corresponding to the reactor as a whole; and PS IV, representing the water that circulates through the heat exchanger for cooling the reactor. The heat removed, represented by  $\dot{Q}$ , is observed to exit from the liquid. However, due to the assumption of thermal equilibrium, it is presumed the same temperature in both the gas and liquid phases. The PS IV is not used to present the balance equations forming the basic structure of the model, but it is shown here for completeness. Stream 18 represents the flow of condensed liquid from the vapour phase, while stream 19 represents the flow of vapour transitioning from the liquid to the gas-vapour phase at the top of the reactor.

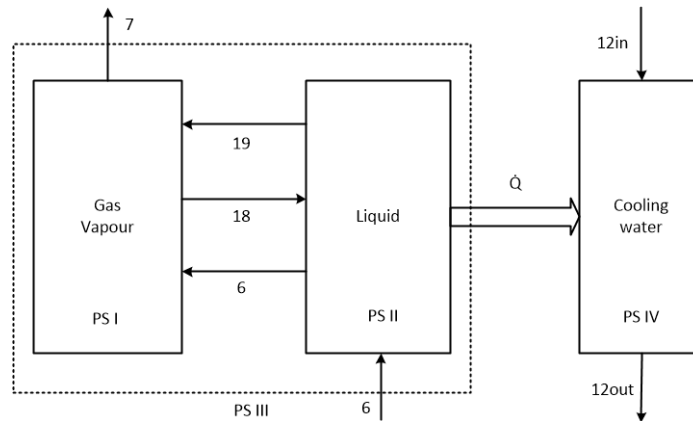


**Fig. 2** PSs defined for modelling the reactor.

### 3 Model construction

In this section, the set of steps 4 to 7 of the methodology for PBSM (Lema-Perez et al., 2019), called model construction, is applied to the TE process. These four steps include the conservation principle application, the definition of the model basic structure, the recognition of variables, structural parameters, and structural constants, and the determination of constitutive and assessment equations. This paper follows the recommendation of Ricker and Lee (1995b) in terms of reproducing the essential characteristics of the process without introducing unnecessary complexity. For this reason, energy balances are not included in the model, and equipment temperatures (except the condenser and flash separator temperature) are treated as controlled variables, assuming there are suitable temperature control loops operating in the real plant.

#### 3.1 Reactor submodel construction

##### 3.1.1 Conservation principle application

In this step, dynamic material balances are applied to the PSs of interest to obtain the basic structure of the model. All material balances in the reactor will be conducted on a molar basis due to the presence of chemical reactions. This approach is easier and more direct than conducting mass balances, which would require using the molecular weights of all compounds to convert moles to mass. On the other hand, although nowadays it is more common to formulate the balances in terms of concentrations, in this paper, the balance in terms of moles is kept. In addition, the molar flow rates, currently represented by  $\dot{n}$ , are indicated here with  $F$ . These two changes on current practice for process modelling are applied here to preserve the integrity of the original benchmark. The previous remark also applies to the other unit operations of the plant.

##### *Gas-vapour phase of the reactor (PS I)*

This PS only considers the gas-vapour contained in the upper part of the reactor. It is assumed that the number of bubbles inside the liquid is quite low and, besides, the

residence time of these bubbles in the liquid is short. Therefore, all the gas can be considered at the top of the reactor.

*Total material balance.* The total material balance equation, in molar units, for the gas-vapour confined in the reactor is

$$\frac{dN_{\text{I}}}{dt} = F_6 - F_7 + \sum_{i=A}^H \sum_{j=1}^3 v_{i,j} r_j + F_{19} - F_{18}, \quad (4)$$

where  $N_{\text{I}}$  are the total moles of gas and vapour contained in the PS I,  $F_k$  represents the molar flow rate in stream  $k$ ,  $v_{i,j}$  is the stoichiometric coefficient of compound  $i \in \{A, B, \dots, H\}$  in reaction  $j \in \{1, 2, 3\}$ . Finally,  $r_j$  is the rate of the reaction  $j$ . Equation (4) highlights the necessity of considering both liquid and vapour flows to maintain the equilibrium of volatile substances (D, E, F, G, and H) between the two phases in the reactor. This fact may be why Downs and Vogel's proposal does not account for separate PSs, but instead focuses on the reactor as a whole (PS III), as depicted below. While (4) remains valid, its evaluation is more complex than determining the change in moles in the gas-vapour phase as the sum of individual changes for each species. Thus, such a calculation will be performed using the component balances outlined in the following sections.

*Component material balance.* The component material balance equation for the gas-vapour contained in the reactor is

$$\frac{dN_{i,\text{I}}}{dt} = y_{i,6} F_6 - y_{i,7} F_7 + \sum_{j=1}^3 v_{i,j} r_j \pm F_{i,18-19}, \quad (5)$$

where  $N_{i,\text{I}}$  are the moles of compound  $i$  in PS I,  $y_{i,k}$  is the molar fraction of component  $i$  in stream  $k$  and  $F_{i,18-19}$  represents the net equilibrium molar flow of species  $i$  between the liquid and the gas-vapour. Equation (5) also remains valid, but it requires the calculation of the parameter  $F_{i,18-19}$ . The sign of this parameter must be determined during its calculation. To avoid the evaluation of this parameter, which implies iteration and affects the gas-vapour concentrations modifying the reaction kinetics, the approach is to first assess the effect of the chemical reactions in the reactor as a whole. Subsequently, the equilibrium calculation is applied to determine the change in moles in each phase after the reactions.

### ***Liquid phase of the reactor (PS II)***

This PS only considers the liquid contained in the lower part of the reactor. It should be noted that stream 6 consists mostly of permanent gases (A, B, and C), but it also contains condensable substances that enter the reactor as vapours at the feed temperature. This fact allows for the assumption that the feed, although it bubbles in the liquid, immediately transitions into the gas-vapour phase, from which the liquid-vapour equilibrium is established.

*Total material balance.* The total material balance equation, in molar units, for the liquid contained in the reactor is

$$\frac{dN_{\text{II}}}{dt} = F_{18} - F_{19}, \quad (6)$$

remembering that streams 18 and 19 represent molar flows established between the liquid and vapour phases to maintain the thermodynamic equilibrium.

*Component material balance.* The component material balance equation for the liquid inside the reactor can be just written as

$$\frac{dN_{i,\text{II}}}{dt} = \pm F_{i,18-19}. \quad (7)$$

### ***Reactor as a whole (PS III)***

From the previous balances, it is evident that the information obtained from them implies iterations that complicate the solution of the model equations. Perhaps that is why the model equations presented by [Ricker and Lee \(1995b\)](#) allude to molar balances in the reactor as a whole.

*Total material balance.* This balance does not distinguish whether the reactions occur in the gas phase or the liquid phase. Instead, it considers the moles in the entire reactor, regardless of the phases, and includes only input and output streams. The general balance of moles in the reactor, viewed as a whole, is as follows:

$$\frac{dN_{\text{III}}}{dt} = F_6 - F_7 + \sum_{i=A}^H \sum_{j=1}^3 v_{i,j} r_j, \quad (8)$$

with  $N_{\text{III}}$  being the total moles contained in PS III. Although (8) allows for the calculation of these moles, having both the moles of gas-vapour and those of liquid  $N_{\text{III}}$  is of limited utility when the calculation of the reaction kinetics requires the value of the moles contained only in the gas-vapour phase  $N_{\text{I}}$ .

*Component material balance.* Similarly to the total material balance, the component material balance is as follows:

$$\frac{dN_{i,\text{III}}}{dt} = y_{i,6} F_6 - y_{i,7} F_7 + \sum_{j=1}^3 v_{i,j} r_j. \quad (9)$$

Notice that for species B the chemical reaction term is equal to zero all the time, since it is an inert species.

### **3.1.2 Submodel basic structure**

The basic structure of the reactor submodel comprises essential equations to address the defined modelling objective. In this regard, the only expression that provides relevant information is (9). However, it is important to highlight that this expression generates eight equations, corresponding to each compound  $i$  involved in the process.

### 3.1.3 Variables, structural parameters, and structural constants

The model includes variables, parameters, and constant values. Variables are those solved within the model, with their values determined after solving the set of differential equations. Parameters are values required by the model to be solved. Moreover, constants are universal known values or values set by the modeller for the specific application. In that sense, the reactor model variables are  $N_{i,III}$ , the structural parameters are  $y_{i,6}$ ,  $y_{i,7}$ ,  $F_6$ ,  $F_7$ , and  $r_j$ . Besides, the model constants are the stoichiometric coefficients  $v_{i,j}$ . All of these parameters are referred to as structural parameters since they are directly observable in the basic structure of the model, unlike functional parameters, which belong to the constitutive and assessment equations of the extended structure of the model. Finally, considering the eight substances involved in the process and the three chemical reactions, there are a total of eight variables, 21 structural parameters, and 24 constants.

### 3.1.4 Constitutive and assessment equations

This step involves establishing constitutive or assessment equations to determine the majority of structural parameters. Parameters lacking such equations must be derived from experimental data or derived from a correlation submodel. The remaining structural parameters have straightforward assessment equations as they are directly extracted from process operation data. A constitutive equation for a parameter can generate additional parameters, which must also be defined. When a function is used to determine a parameter, the resulting parameters are called functional parameters. The new function becomes part of the model extended structure, and the newly generated parameters should be promptly specified to elucidate the solution sequence of the original parameters. In general, in this paper, the initial values for the parameters should be sourced from the referenced articles. For the base case of plant operation, the study by [Downs and Vogel \(1993\)](#) is enough, while for other operation modes, the parameters should be computed using data from both the aforementioned work and that by [Ricker and Lee \(1995b\)](#), as will be seen in Section 5. Finally, the constitutive and assessment equations for the reactor model are presented below.

#### *Molar fractions $y_{i,6}$ and $y_{i,7}$*

The molar fraction at the reactor inlet is derived from the mixing point model (as presented in the supplementary material). On the other hand, the molar fraction at the reactor outlet is calculated as follows:

$$y_{i,7} = \frac{P_{i,R}}{P_R}, \quad (10)$$

being  $P_{i,R}$  the partial pressure of compound  $i$  at the top of the reactor and  $P_R$  the absolute pressure inside the reactor. The functional parameters derived from (10) must be determined. Thus,  $P_R$  is calculated as the sum of the partial pressures of each

compound  $P_{i,R}$ , following the calculation sequence:

$$P_{i,R} = \frac{N_{i,I} R T_R}{V_g}, \quad i = A, B, C, \quad (11)$$

$$P_{i,R} = \gamma_{i,R} x_{i,II} P_{i,R}^{sat}, \quad i = D, E, F, G, H, \quad (12)$$

$$P_R = \sum_{i=A}^H P_{i,R}, \quad i = A, B, C, D, E, F, G, H, \quad (13)$$

where  $R$  is the universal gas constant,  $T_R$  is the absolute temperature inside the reactor, which is a parameter of fixed value taken directly from process operation data. Moreover,  $V_g$  is the volume of the gas phase in the reactor and  $\gamma_{i,R}$ ,  $x_{i,II}$ , and  $P_{i,R}^{sat}$  are the activity coefficient, the liquid phase molar fraction, and the saturation pressure (evaluated at  $T_R$ ) of substance  $i$  in the reactor, respectively. Within the reactor, both liquid and gas phases are present and an equilibrium between these phases needs to be described. For the non-condensable components A, B, and C, the ideal gas equation (11) is used to determine their partial pressure at the reactor head. Instead, since the liquid phase of the reactor deviates from ideal behaviour, it is essential to account for its intermolecular interactions. To address this issue, the modified Rault's law (12) is applied.

The saturation pressure is determined as

$$P_{i,R}^{sat} = 10^{-3} \exp \left( a_i + \frac{b_i}{c_i + T_R} \right), \quad (14)$$

with  $a$ ,  $b$ , and  $c$  being the Antoine constants (known values) for component  $i = D, E, F, G$ , and  $H$ . The molar fraction of the compounds in the liquid phase of the reactor is calculated as

$$x_{i,II} = \frac{N_{i,II}}{N_{II}} = \frac{N_{i,II}}{\sum_{i=D}^H N_{i,II}}. \quad (15)$$

Finally, the volume of the gas phase of the reactor, namely  $V_g$ , must be found. For such a calculation, it is necessary to determine the volume of the liquid phase  $V_L$  of the reactor, as follows:

$$V_L = \frac{N_{II}}{\rho_{L,R}}, \quad (16)$$

where  $\rho_{L,R}$  represents the molar density, computed as the weighted average of the densities of the substances in the reactor liquid based on their molar fraction. The densities of individual compounds are provided with specific values in the seminal paper. Finally, given that the total volume of the reactor  $V_R$  remains constant, the volume of the gas phase can be readily calculated by taking the difference

$$V_g = V_R - V_L. \quad (17)$$

### Molar flow rates $F_6$ and $F_7$

The molar flow rate at the reactor inlet  $F_6$  is calculated using specific parameters for the mixing point process system (see supplementary material). On the other hand, the molar flow rate at the reactor outlet,  $F_7$ , is determined from a useful expression provided by [Jockenhövel et al. \(2003\)](#), as follows:

$$F_7 = 1.5355 \sqrt{P_R - P_{sep}}, \quad (18)$$

which gives the result in kmol/s as long as the pressure values are expressed in MPa. Equation (18) is a typical pressure gradient flow equation through a valve or pipe section.

**Remark 3.** *Although the authors adjusted the coefficient value to match the base case, it is important to note that this coefficient is inherent to a device or a pipe, rather than the specific operating conditions. Therefore, this expression was used for all operation modes in this paper.*

### Reaction rates $r_j$

The reaction rates are determined using constitutive equations, which are empirically derived and possess a non-elementary structure. These equations were reported by [Ricker and Lee \(1995b\)](#) and are provided next:

$$r_1 = \alpha_1 V_g \exp \left[ -44.06 + \frac{42600}{R_k T_R} \right] P_{A,R}^{1.08} P_{C,R}^{0.311} P_{D,R}^{0.874}, \quad (19)$$

$$r_2 = \alpha_2 V_g \exp \left[ -10.27 + \frac{19500}{R_k T_R} \right] P_{A,R}^{1.15} P_{C,R}^{0.370} P_{E,R}^{1.00}, \quad (20)$$

$$r_3 = \alpha_3 V_g \exp \left[ -59.50 + \frac{59500}{R_k T_R} \right] P_{A,R} (0.77 P_{D,R} + P_{E,R}), \quad (21)$$

where  $\alpha_1$ ,  $\alpha_2$ , and  $\alpha_3$  are the dimensional factors of the reaction and  $R_k$  is the universal gas constant (see Remark 5).

**Remark 4.** *The signs inside the square brackets were inverted, since using the expressions given by Ricker and Lee yielded unexpectedly deviant results. This discrepancy could suggest a possible typing error in the mentioned paper.*

**Remark 5.** [Ricker and Lee \(1995b\)](#) noted that a different value of this constant is utilized for the kinetics of chemical reactions, as it is expressed in different units:  $R_k = 1.987 \frac{\text{cal}}{\text{gmol-K}}$ .

## 3.2 Basic structure of the TE model

Table 1 summarizes both the basic structure and the constitutive and assessment equations corresponding to the other process equipment. For further details, the reader is referred to the supplementary material, which includes the deduction of these equations as well as additional observations and relevant discussions that support their formulation. To conclude the model construction section, the basic structure of the complete TE model is formed by (9), (22), (23), (24), and (25).

**Table 1:** Equations corresponding to the other process equipment.

Process system	Equations
PS X: Condenser and flash separator as a whole	$\frac{dN_{i,X}}{dt} = y_{i,7} F_7 - y_{i,17} F_{17} - x_{i,10} F_{10} \quad (22)$ $y_{i,17} = \frac{P_{i,sep}}{P_{sep}}$ $x_{i,10} = \frac{N_{i,VI}}{N_{VI}} = \frac{N_{i,VI}}{\sum_{i=D}^H N_{i,VI}}$ $F_{17} = F_7 - F_{10}$
PS XI: Gas-vapour phase of the stripper	$\frac{dN_{i,XI}}{dt} = y_{i,4} F_4 + \phi_i (x_{i,10} F_{10} + y_{i,4} F_4) - y_{i,5} F_5 \quad (23)$ $y_{i,5} = \frac{N_{i,XI}}{N_{XI}}$ $F_5 = F_{10} + F_4 - F_{11} - \sum_{i=G}^H \frac{dN_{i,str}}{dt}$ $\phi_i = \frac{y_{i,5} F_5 - y_{i,4} F_4}{x_{i,10} F_{10} + y_{i,4} F_4}$
PS XII: Liquid phase of the stripper	$\frac{dN_{i,XII}}{dt} = x_{i,10} F_{10} - \phi_i (x_{i,10} F_{10} + y_{i,4} F_4) - x_{i,11} F_{11} \quad (24)$ $x_{i,11} = \frac{N_{i,XII}}{N_{XII}}$
PS XIV: Mixing point	$\frac{dN_{i,XIV}}{dt} = y_{i,1} F_1 + y_{i,2} F_2 + y_{i,3} F_3 + y_{i,5} F_5 + y_{i,8} F_8 - y_{i,6} F_6 \quad (25)$ $y_{i,6} = \frac{N_{i,XIV}}{N_{XIV}}$ $F_8 = F_{17} - F_9$ $F_6 = F_1 + F_2 + F_3 + F_5 + F_8$

## 4 Model validation

In this section, the set of the last three steps, 8 to 10, of the methodology for PBSM, called model validation, is applied to the TE process. As these three steps indicate the verification of degree of freedom, the computational model construction, and the results validation from real data of the process, they are discussed as a whole for the pieces of equipment forming the plant.

### 4.1 Degrees of freedom analysis

To ascertain whether the mathematical model can be solved, it is essential to ensure that the number of model unknowns (encompassing variables and structural and functional parameters) matches the number of equations, resulting in zero degrees of freedom (DoF) for the model. In this regard, the TE model developed comprises a total of 239 unknowns, distributed as follows: 40 variables, 110 structural parameters, and 89 functional parameters. Additionally, it can be confirmed that all equations necessary to solve the model were elucidated during its construction (Section 3). Thus,

the degrees of freedom are zero ( $\text{DoF} = 239 - 239 = 0$ ). Apparently, the fact of adding new equations (e.g., control laws for potential controllers) in the simulator modifies the model degrees of freedom. However, these degrees of freedom were considered in the calculation performed in step 7 of the modeling methodology when all new control actions are taken as known values. Hence, the benchmark users are able to introduce in the simulator the control law they consider most appropriate for their current application without affecting the model structure.

## 4.2 Computational model construction

This section involves creating a computational model, specifically, a computer program capable of solving the model equations without deviating from the true mathematical model response. Thus, the computational model was programmed and numerically solved in Python using the Euler method with a 0.001 hours (3.6 s) fixed step, which is a small enough step to capture the system dynamic. On the other hand, it should be noted that the input data provided to the plant for the model solution contains finite decimals. However, Python's default calculation precision extends up to 28 decimal places, which may result in instability during convergence of the method and deviation from the steady-state conditions due to the accumulation of small errors in the differential terms. Therefore, it is advisable to limit the number of decimal places in Python or appropriately round the differential terms in the Euler method. The latter approach was adopted to ensure the maintenance of steady-state conditions throughout the process given in the seminal paper ([Downs and Vogel, 1993](#)). For this particular study, it is recommended to round numbers up to three decimal places if they are greater than one and up to three significant figures if they are less than one.

## 4.3 Results validation

This section presents some of the results achieved after solving the computational model. It is recalled that the primary goals of this study were to comprehensively deduce the TE model using a PBSM approach and obtain the parameters values to accurately simulate the steady-state conditions of all the operation modes reported by [Ricker and Lee \(1995b\)](#), Table 4. Although it was possible to simulate the open-loop steady-state values of all operation modes, given the complex behaviour and high sensitivity of the plant, it was necessary to implement some PID controllers to evaluate the effect of certain disturbances and observe the system responses. Therefore, the five control loops suggested by [Andersen et al. \(2021\)](#) were adopted as the minimum necessary to maintain the stability of the plant against small disturbances. The controlled variables included the pressure, temperature, and level in the reactor, as well as the level in the flash separator and the level in the stripping tower. Likewise, the manipulated variables comprised the purge flow, the cooling water flow in the reactor, the temperature in the flash separator, the liquid flow out of the separator, and the liquid flow out of the stripping tower, respectively. For each of the operation modes, it was necessary to retune the PID controller parameters, further demonstrating the control challenge that this benchmark represents. Moreover, it is highlighted that this parameters were arbitrarily tuned solely to achieve stable behaviour. Thus,

this approach does not represent an optimal or advanced control strategy, as it falls outside the scope of this study. For more detailed exploration of advanced control strategies, readers are encouraged to consult multiple control works focusing on the TE benchmark (Zerkaoui et al., 2010; Budman et al., 2008; Lawrence Ricker, 1996).

Figures 3, 4, 5, and 6 show some of the results obtained for the operation base case, mode 1, mode 2, and mode 3, respectively. The initial steady-state values are displayed for up to 10 hours of operation, followed by the response to a disturbance. The starting points of the curves representing the moles of key substances correspond to inventory values of each piece of equipment. The dynamic transitions presented in such figures exhibit smooth, natural, and bounded behaviour, consistent with expected physical trends. The simulator accurately reproduces the actual process values with minimal error. Table 2 shows the steady-state relative errors of key variables, including the average and maximum errors across the four operating modes, offering further insights into the model accuracy.

**Table 2** Steady-state relative errors (%) of the value of moles of key compounds and the reactor pressure.

Variable	Base case	Mode 1	Mode 2	Mode 3	Maximum error	Average error
A in reactor	0,46	0,18	0,79	0,22	0,79	0,41
A in flash separator	0,09	0,11	1,75	0,12	1,75	0,52
C in reactor	0,57	0,36	0,97	0,41	0,97	0,58
C in flash separator	0,26	0,22	0,04	0,02	0,26	0,14
G in reactor	0,37	0,26	2,02	0,55	2,02	0,80
G in flash separator	6,01	5,69	9,73	6,20	9,73	6,91
H in reactor	0,67	0,61	0,77	0,38	0,77	0,61
H flash separator	9,12	8,28	11,32	2,98	11,32	7,93
Reactor pressure	3,75	3,65	3,54	3,74	3,75	3,67

As energy balances were omitted from this study, the controlled reactor temperature is not depicted, as it was maintained at a constant value to simulate the operation of a finely tuned PID controller. This approach is justified because the manipulated variable, the cooling water flow, is a parameter that does not interact with other parameters of the plant. Thus, modelling the behaviour of this parameter is unnecessary.

Unfortunately, real simulations using the original Downs and Vogel simulator were not feasible because that software is no longer publicly available. Nevertheless, Figure 7 shows the agreement between our derived model and the updated simulator of Bathelt et al. (2015), comparing the responses of three measured variables (XMEAS (23), XMEAS (31), XMEAS (40)) to three representative faults (IDV (1), IDV (2), IDV (3)) reported in the seminal paper (Downs and Vogel, 1993). Although Ricker’s simulator operates in closed loop, whereas our derived model runs in open loop (retaining only the necessary controllers for stability), both show alignment of initial conditions and convergence of process outputs toward similar steady states, supporting the validity of our derived model.

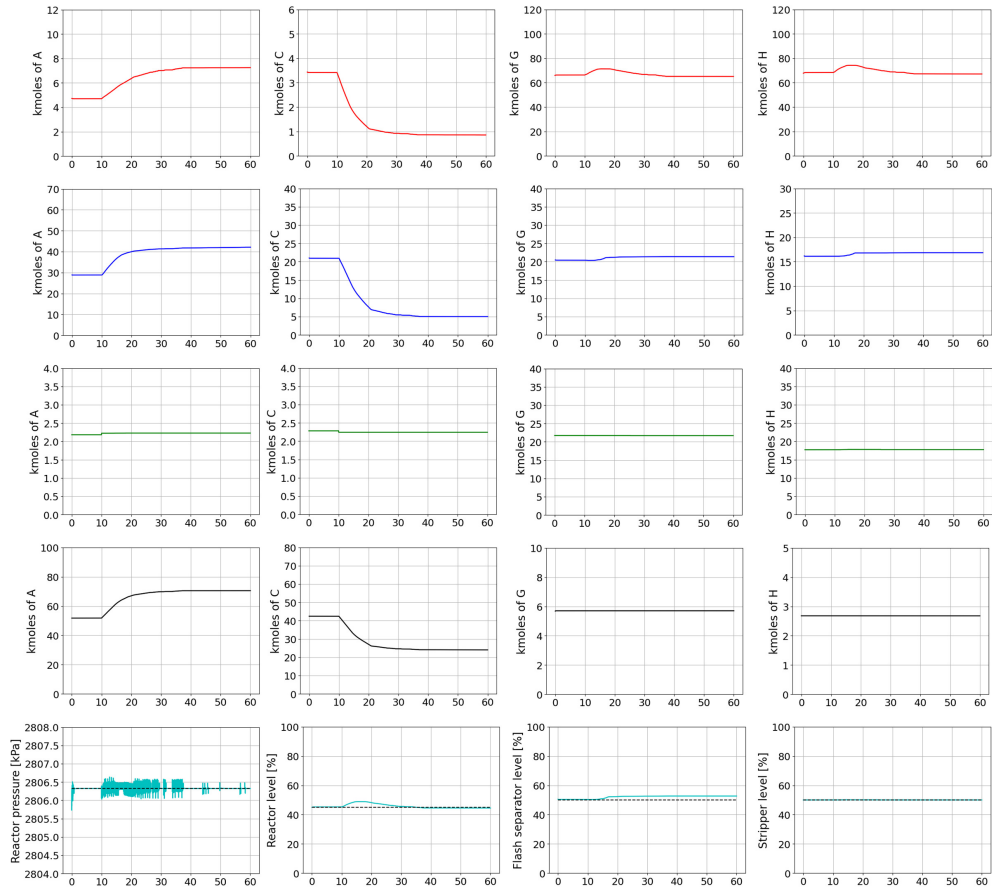


**Fig. 3** Base case. Some process responses to a step disturbance in stream 4 ( $y_{A,4}$  about +2% and  $y_{C,4}$  about -2%) at  $t=10$  hours. Reactants A and C are shown in the gas phase while products G and H are shown in the liquid phase (except at the mixing point, where all species are gases). First row: reactor, second row: flash separator, third row: stripper, fourth row: mixing point and, fifth row: controlled variables (the black dashed line corresponds to the variable set-point). The x-axis shows the time in hours in all plots.

## 5 Initial conditions and parameters values

The final part of this paper aims to provide all the necessary information for interested researchers to simulate the four basic operation modes of the TE plant. Although the model has already been deduced above, having the process initial conditions and the parameters values is essential for replicating the results obtained and utilizing the benchmark with a greater understanding of the process. Data not presented here can be found in the seminal article by [Downs and Vogel \(1993\)](#) along with that by [Ricker and Lee \(1995b\)](#). This section details how the initial conditions (steady-state values) for the TE plant model are calculated or where they can be accessed. In each instance, it is clarified the source of the direct data to be taken or the data used for the calculation. For this purpose, the source table number is provided along with the corresponding

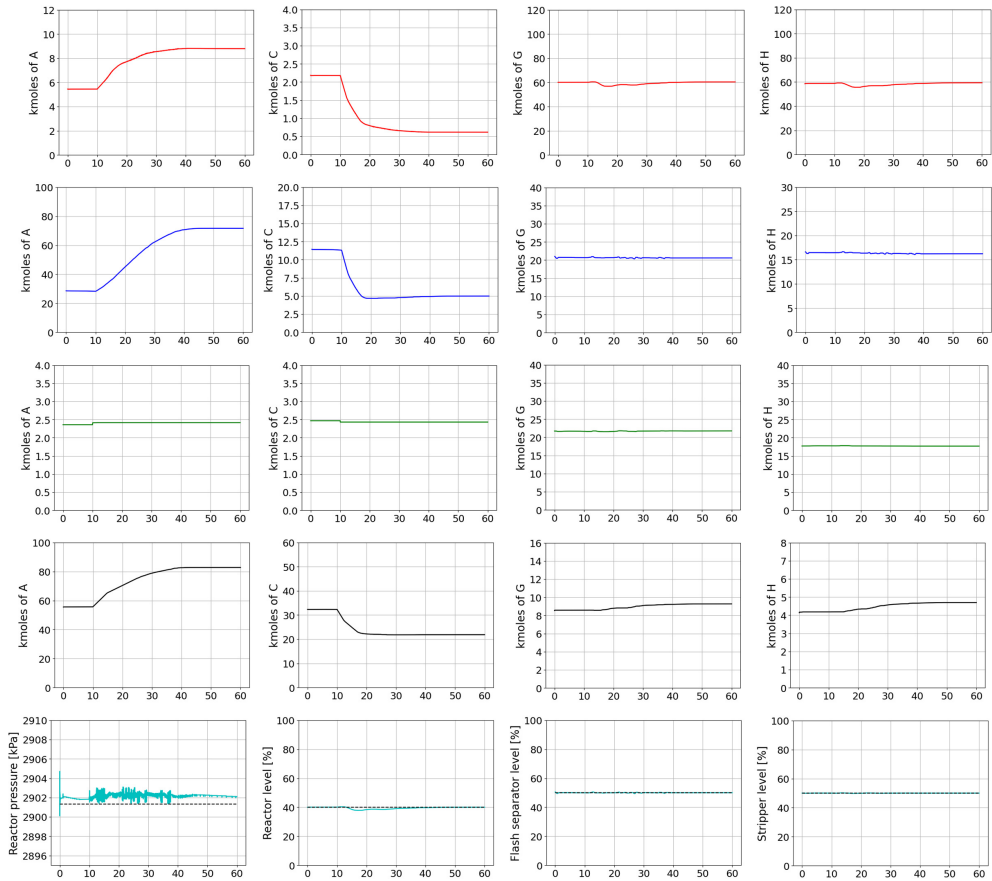


**Fig. 4** Mode 1. Some process responses to a step disturbance in stream 4 ( $y_{A,4}$  about +2% and  $y_{C,4}$  about -2%) at  $t=10$  hours. Reactants A and C are shown in the gas phase while products G and H are shown in the liquid phase (except at the mixing point, where all species are gases). First row: reactor, second row: flash separator, third row: stripper, fourth row: mixing point and, fifth row: controlled variables (the black dashed line corresponds to the variable set-point). The x-axis shows the time in hours in all plots.

reference. When discrepancies arise in the values, either due to differences in the sources or because these discrepancies became evident during the adjustment of the computational model, it is specified which value to use. Moreover, although the values utilized in this section correspond to the base case of plant operation, the analysis remains similar for determining the initial conditions of the other operation modes, taking advantage of the operation data (parameters values) that will be given at the end of this paper (see appendix A).

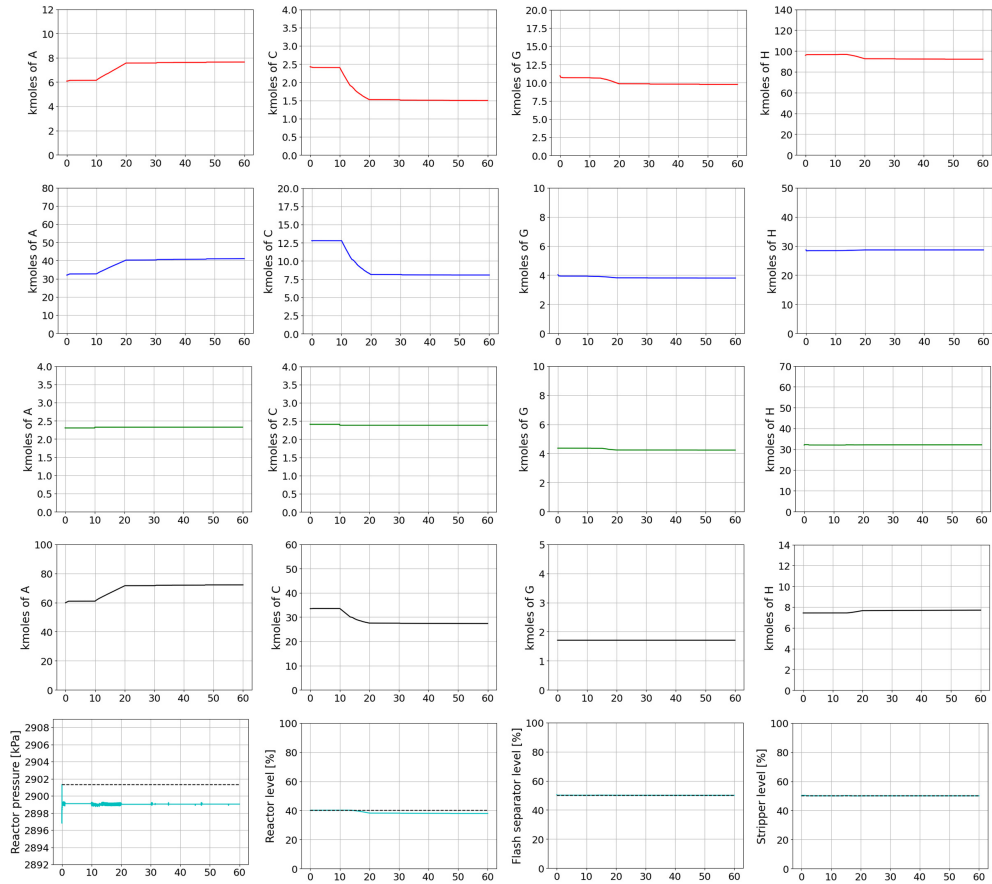


**Fig. 5** Mode 2. Some process responses to a step disturbance in stream 4 ( $y_{A,4}$  about +1.2% and  $y_{C,4}$  about -1.2%) at  $t=10$  hours. Reactants A and C are shown in the gas phase while products G and H are shown in the liquid phase (except at the mixing point, where all species are gases). First row: reactor, second row: flash separator, third row: stripper, fourth row: mixing point and, fifth row: controlled variables (the black dashed line corresponds to the variable set-point). The x-axis shows the time in hours in all plots.

## 5.1 Reactor

### *Volume of the phases*

This calculation involves first finding the total volume of the reactor. For this, the volume of liquid in the reactor,  $V_L = 16.55 \text{ m}^3$  ((Downs and Vogel, 1993), Table 1), and the percentage of liquid level within the reactor,  $L_{III} = 75\%$  ((Downs and Vogel, 1993), Table 4), are used. Considering that nothing is mentioned in the seminal paper, it is assumed that the volume change between the lid and bottom of the reactor, even if they are torispherical, is equivalent to that of a cylinder with plane lid and bottom.

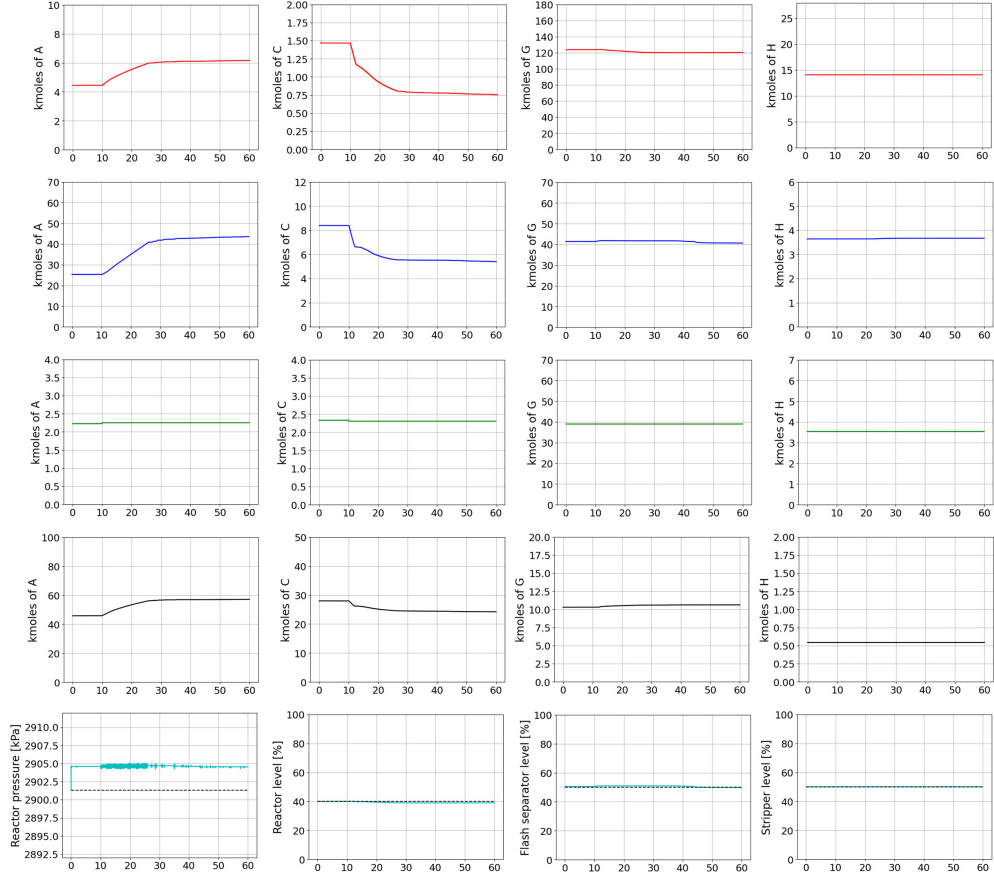


**Fig. 6** Mode 3. Some process responses to a step disturbance in stream 4 ( $y_{A,4}$  about +1.4% and  $y_{C,4}$  about -1.4%) at  $t=10$  hours. Reactants A and C are shown in the gas phase while products G and H are shown in the liquid phase (except at the mixing point, where all species are gases). First row: reactor, second row: flash separator, third row: stripper, fourth row: mixing point and, fifth row: controlled variables (the black dashed line corresponds to the variable set-point). The x-axis shows the time in hours in all plots.

Consequently, the total volume of the reactor can be determined as

$$V_R = \frac{V_L}{\frac{L_{III}}{100}} = \frac{16.55 \text{ m}^3}{\frac{75}{100}} = 22.07 \text{ m}^3.$$

This value for the total reactor volume deduced from the original data differs from that provided by [Ricker and Lee \(1995b\)](#) ( $V_R = 36.8 \text{ m}^3$ ). After running the computational model, a significant discrepancy is observed in the steady-state molar fractions. Thus, the previous value will be considered as valid, i.e.,

$$V_R = 36.8 \text{ m}^3 \rightarrow \text{True value.}$$

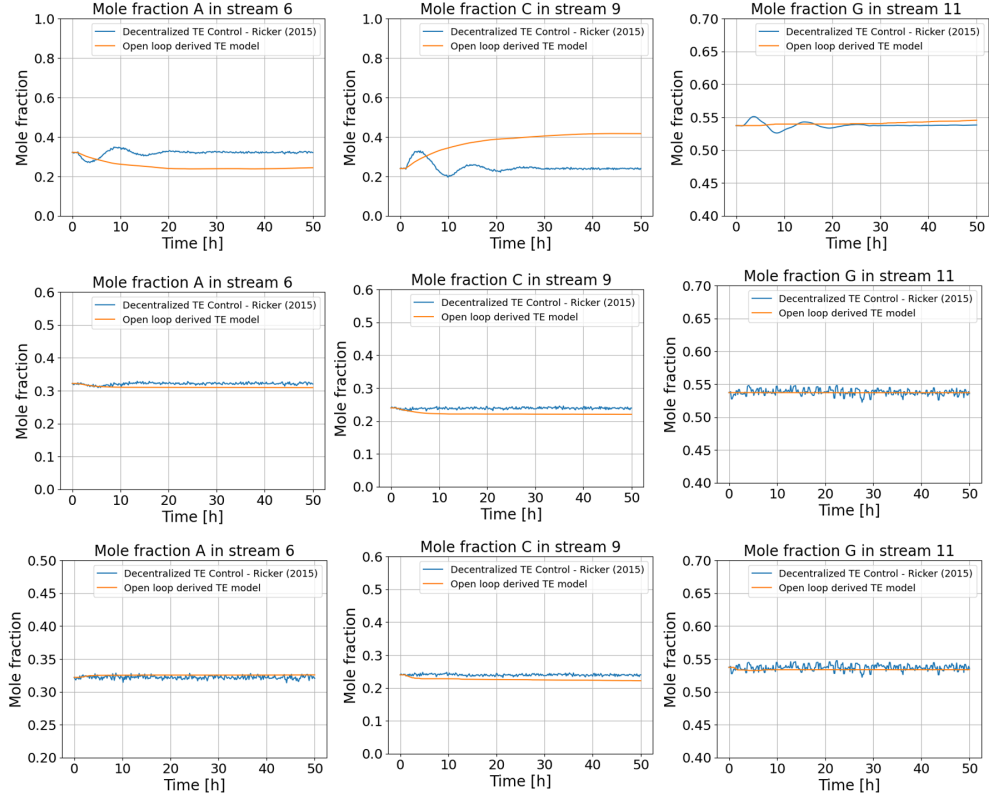


**Fig. 7** Dynamic responses of three measured variables to three process faults. Columns 1, 2, and 3 correspond to the measured variables XMEAS (23), XMEAS (31), and XMEAS (40), respectively. Likewise, rows 1, 2, and 3 correspond to the faults IDV (1), IDV (2), and IDV (3), respectively. The faults are introduced after 1 hour of operation and simulating the base case of plant operation.

From the total volume of the reactor, the volumes of the liquid phase and the gas-vapour phase can be determined as

$$V_L = V_R \frac{L_{III}}{100} = 36.8 \text{ m}^3 \frac{75}{100} = 27.6 \text{ m}^3,$$

$$V_g = V_R \frac{100 - L_{III}}{100} = 36.8 \text{ m}^3 \frac{(100 - 75)}{100} = 9.2 \text{ m}^3.$$

Using these values in the computational model, it is not possible to equate the initial pressure with the sum of the partial pressures of the compounds in the gas-vapour phase. Therefore, the percentage of liquid level must be adjusted, resulting in a value of

$$L_{III} = 45\% \rightarrow \mathbf{True\ value.}$$

Finally, the volumes of the phases within the reactor are

$$V_L = 16.56 \text{ m}^3 \rightarrow \mathbf{True\ value,}$$

$$V_g = 20.24 \text{ m}^3 \rightarrow \text{True value.}$$

**Remark 6.** *It is highlighted that the value of the liquid volume in reactor ( $V_L = 16.56 \text{ m}^3$ ) coincides with that given by [Downs and Vogel \(1993\)](#) in their Table 1, which may suggest that the error is when in Table 4 the authors set the liquid level in the reactor at 75%, quite different from the adjusted value of 45%.*

#### ***Moles of each substance in the gas-vapour***

First, the total moles in the gas-vapour phase of the reactor should be calculated. This step is achieved by utilizing the total moles in the reactor for each substance as provided in ([Ricker and Lee, 1995b](#)), Table 4, along with the molar fraction of the respective substance in that phase, which can be considered as the same as in stream 7, given in ([Downs and Vogel, 1993](#)), Table 1. It is important to note that this analysis is valid for substances that are considered permanent gases, namely, A, B, and C. For instance, utilizing the data for compound A,

$$N_I = \frac{N_{A,I}}{y_{A,7}} = \frac{4.72200}{0.27164} = 17.38330 \text{ kmol.}$$

Another method to calculate the total moles in the gas-vapour phase of the reactor is by employing the ideal gas equation, utilizing the other known data: absolute pressure ( $P_R = 2806.325 \text{ kPa}$ ), absolute temperature ( $T_R = 393.55 \text{ K}$ ), gas universal constant ( $R = 8.314 \frac{\text{kJ}}{\text{kmol}\cdot\text{K}}$ ), and the gas-vapour volume previously deduced ( $V_I = 20.24 \text{ m}^3$ ). Thus, adding appropriate unit conversion factors, the following value is obtained:

$$N_I = \frac{2806.325 \cdot 1000 \frac{\text{kg}}{\text{m}\cdot\text{s}^2} \cdot 20.24 \text{ m}^3}{8.314 \frac{1000 \text{ kg}\cdot\text{m}^2}{\text{kmol}\cdot\text{K}} \cdot 393.55 \text{ K}} = 17.35955 \text{ kmol.}$$

Although this value differs slightly from the one calculated previously, it still serves as a right estimate and corroborates the value determined for the volume of the gas-vapour phase. Finally, to determine the moles of each of the substances, the molar fraction of stream 7 provided as data for the base case (([Downs and Vogel, 1993](#)), Table 1) is utilized in the following way:

$$N_{i,I} = y_{i,7} N_I. \quad (26)$$

The results obtained are presented in Table 3, with the initial three quantities (A, B, and C) corresponding with those provided for the base case (([Ricker and Lee, 1995b](#)), Table 4). In addition, the current work reports the values for the other substances that were not reported in the previously cited table.

#### ***Moles of each substance in the liquid***

Substances A, B, and C are considered permanent gases. Hence, it is assumed that they are not present in the liquid phase. Consequently, the moles of the substances in

**Table 3** Initial moles in the reactor gas-vapour phase (all units are kmol).

Substance	Base case	Mode 1	Mode 2	Mode 3
A	4.72234	5.45360	6.08990	4.45490
B	1.98062	3.60915	1.95681	7.20843
C	3.43571	2.18343	2.43230	1.47431
D	0.18688	0.15022	0.02219	0.36254
E	3.08089	2.93026	4.11742	0.73260
F	0.37533	1.01909	1.35652	0.33846
G	2.13864	2.52035	0.50218	4.65059
H	1.46430	1.65534	2.91363	0.35634

the liquid phase (D through H) can be directly inferred from (Ricker and Lee, 1995b), Table 4. On the other hand, according to assumption A9 given by Ricker and Lee (1995b), the accumulation of the less volatile components in the gas-vapour phase is also neglected. These components have an equilibrium partial pressure, but the corresponding number of moles in the vapour is neglected when computing the molar holdups. The preceding statement applies similarly to the flash separator as well.

**Remark 7.** *Although the previous simplification is implemented to avoid iterative flash calculations, it is worth noting that the substances D through H, which are neglected in the gas phase, collectively constitute approximately 42% of the total moles in this phase (value for the base case).*

#### Reaction rates $r_j$

To determine the values of the reaction rate at steady-state, it is enough to set the derivatives to zero in the equation of the model basic structure (9). For example, using the equations for compounds D, G, and H and substituting the molar fractions and flow rates (known data), the values of the three reaction rates can be obtained from the following  $3 \times 3$  algebraic system:

$$\begin{aligned} 0 &= y_{D,6} F_6 - y_{D,7} F_7 - 1 r_1 - 1 r_3, \\ 0 &= y_{G,6} F_6 - y_{G,7} F_7 + 1 r_1, \\ 0 &= y_{H,6} F_6 - y_{H,7} F_7 + 1 r_2. \end{aligned}$$

#### Reaction factors $\alpha_j$

With the reaction rates values at steady-state already calculated, the expressions for the reaction rates can be utilized to find the value of the reaction factor for each reaction. For instance, considering the first reaction,

$$\alpha_1 = r_1 \left[ V_g \exp \left( -44.06 + \frac{42600}{R_k T_R} \right) p_{A,R}^{1.08} p_{C,R}^{0.311} p_{D,R}^{0.874} \right]^{-1}, \quad (27)$$

where the partial pressures of the compounds  $P_{i,R}$  in the reactor gas-vapour phase can be found from the definition, as follows:

$$P_{i,R} = y_{i,T} P_R. \quad (28)$$

### **Activity coefficients $\gamma_i$**

As the main assumption to calculate the substances hold-ups indicates that the permanent gases are only in the gas phase and the condensables are present only in the liquid phase, from (Ricker and Lee, 1995b), Table 4, the initial total moles in the liquid phase can be determined by summing the moles of the individual liquid substances, that is,

$$N_{II} = N_{D,II} + N_{E,II} + N_{F,II} + N_{G,II} + N_{H,II}, \quad (29)$$

and the liquid molar fractions are obtained from the definition, as follows:

$$x_{i,II} = \frac{N_{i,II}}{N_{II}}. \quad (30)$$

Then, the activity coefficients for liquid substances can be calculated using the expression for the modified Raoult's law (12), given that the other values are already known, i.e.,

$$\gamma_{i,R} = \frac{P_{i,R}}{x_{i,II} P_{i,R}^{Sat}}, \quad i = D, E, F, G, H. \quad (31)$$

## **5.2 Condenser-flash separator**

### **Volume of the gas-vapour phase**

This calculation involves first finding the total volume of the condenser-flash separator. For this purpose, the volume of liquid  $V_{VI} = 4.88 \text{ m}^3$  ((Downs and Vogel, 1993), Table 1) and the percentage of liquid level within the condenser-flash separator  $L_{IX} = 50\%$  ((Downs and Vogel, 1993), Table 4) are used. Again, it is assumed that the volume change at the lid and bottom of the equipment is equivalent to that of a cylinder with straight caps. Therefore, the total volume of the separator can be determined as

$$V_{IX} = \frac{4.88 \text{ m}^3}{\frac{50}{100}} = 9.76 \text{ m}^3.$$

Thus, the volume of the gas phase is the remaining 50% ( $V_V = 4.88 \text{ m}^3$ ). However, these values are adjusted later because, as will be evident, they do not align with the moles calculated for the gas using (Ricker and Lee, 1995b), Table 4.

### **Moles of each substance in the gas-vapour**

First, the total moles in the gas-vapour phase of the condenser-flash separator should be calculated. This is achieved by utilizing the total moles for each substance in this equipment as provided in (Ricker and Lee, 1995b), Table 4, along with the molar fraction of the respective substance in that phase, which can be considered as the

same as in streams 17, 8, and 9, given in (Downs and Vogel, 1993), Table 1. Again, it is important to note that this analysis is valid for substances that are considered permanent gases, namely, A, B, and C. For instance, utilizing the data for compound A,

$$N_V = \frac{N_{A,V}}{y_{A,8}} = \frac{28.89500}{0.32958} = 87.6722 \text{ kmol.}$$

On the other hand, with the value found for the moles in the gas phase and the other known parameters: absolute pressure ( $P_{sep} = 2735.025 \text{ kPa}$ ) and temperature ( $T_{sep} = 353.25 \text{ K}$ ), it is possible to verify the value of the gas phase volume using the ideal gas equation, i.e.,

$$V_V = \frac{N_V R T_{sep}}{P_{sep}} = \frac{87.6721 \text{ kmol} \cdot 8.314 \frac{\text{kg}\cdot\text{m}^2}{\text{s}^2\text{kmol}\cdot\text{K}} \cdot 353.25 \text{ K}}{2735.025 \text{ kPa}} = 94.14 \text{ m}^3.$$

It should be noted that this value differs significantly from the one previously calculated of  $4.88 \text{ m}^3$ . Using the new calculated volume,  $94.14 \text{ m}^3$ , the total volume of the separator would be  $99.02 \text{ m}^3$ , resulting in a liquid level of only about 5%. Since this value for the total volume of the separator is close to that reported by Ricker and Lee (1995b) ( $99.1 \text{ m}^3$ ), the last volume value for the gas phase is left as true,

$$V_V = 94.14 \text{ m}^3 \rightarrow \text{True value.}$$

**Remark 8.** *Considering that the calculated liquid level of 5% is significantly different from the reported values of 50% by both sources (Downs and Vogel, 1993; Ricker and Lee, 1995b), it is inferred that the level was determined by considering only the volume of the flash tank, rather than the combined volumes of both equipment: the condenser and the flash tank (as was done to derive the model equations). The sum of the gas-vapour volumes in the condenser and the flash tank represents the true value of  $94.14 \text{ m}^3$ .*

Finally, to calculate the moles of individual substances in the gas-vapour, the molar fraction of stream 8, as indicated in the base case data ((Downs and Vogel, 1993), Table 1), is employed as

$$N_{i,V} = y_{i,8} N_V. \quad (32)$$

The results are reported in Table 4, where the initial quantities for substances A, B, and C correspond with those listed in the base case ((Ricker and Lee, 1995b), Table 4). Moreover, this study includes the values for the remaining substances that were not previously reported in the cited table.

#### ***Moles of each substance in the liquid***

Again, due to the assumption of A, B, and C only in the gas phase and the condensables only in the liquid phase, the moles of the substances in the liquid phase (D through H) can be directly inferred from (Ricker and Lee, 1995b), Table 4.

**Table 4** Initial moles in the separator gas-vapour phase (all units are kmol).

Substance	Base case	Mode 1	Mode 2	Mode 3
A	28.89500	28.56500	32.03900	25.36500
B	12.11893	18.90408	10.29481	41.04286
C	21.02204	11.43644	12.79636	8.39430
D	1.10204	0.76591	0.11371	1.98477
E	16.28862	13.86473	19.56627	3.58715
F	1.98402	4.82176	6.44629	1.65701
G	4.24684	5.83137	1.15456	8.55818
H	2.01558	2.84606	5.06431	0.45522

**Remark 9.** *It is worth noting that the substances D through H, which are neglected in the gas phase, collectively constitute approximately 29% of the total moles in this phase (example value for the base case).*

### **Activity coefficients $\gamma_i$**

In a similar way to what was done for the reactor, the initial total moles in the liquid phase ( $N_{VI}$ ) can be determined from (Ricker and Lee, 1995b), Table 4, by summing the moles of the individual liquid substances. Then, the liquid molar fractions ( $x_{i,VI}$ ) are obtained from the definition of molar fraction. Finally, the activity coefficients for liquid substances can be calculated using (12), given that the other values are already known, i.e.,

$$\gamma_{i,sep} = \frac{P_{i,sep}}{x_{i,VI} P_{i,sep}^{Sat}}, \quad i = D, E, F, G, H. \quad (33)$$

## **5.3 Stripping tower**

### **Volume of the phases**

Given the volume data for the liquid phase  $V_{XII} = 4.43 \text{ m}^3$  ((Downs and Vogel, 1993), Table 1) and the liquid level percentage  $L_{XIII} = 50\%$  ((Downs and Vogel, 1993), Table 4), the total volume of the stripping tower can be determined as

$$V_{XIII} = \frac{4.43 \text{ m}^3}{\frac{50}{100}} = 8.86 \text{ m}^3.$$

Thus, the volume of the gas phase is the remaining 50%, i.e.,

$$V_{XI} = 4.43 \text{ m}^3 \rightarrow \text{True value.}$$

### **Moles of each substance in the gas-vapour**

Since there is no available data on the accumulation of substances in the gas phase inside the stripper, unlike the reactor and the separator, the total moles in this phase can be computed using the ideal gas equation. All other required data is known: absolute pressure ( $P_{str} = 3203.525 \text{ kPa}$ ) and temperature ( $T_{str} = 338.85 \text{ K}$ ) in the stripper,

and the volume previously determined. The calculation is performed as follows:

$$N_{\text{XI}} = \frac{3203.525 \cdot 1000 \frac{\text{kg}}{\text{m}^3} \times 4.43 \text{ m}^3}{8.314 \frac{1000 \frac{\text{kg} \cdot \text{m}^2}{\text{s}^2}}{\text{kmol} \cdot \text{K}} \times 338.85 \text{ K}} = 5.0375 \text{ kmol}.$$

Then, to determine the moles of each of the substances, the molar fraction of stream 5 provided as data for the base case ((Downs and Vogel, 1993), Table 1) is employed in the following way:

$$N_{i,\text{XI}} = y_{i,5} N_{\text{XI}}. \quad (34)$$

The results obtained are presented in Table 5, with the observation that none of these values were reported in (Ricker and Lee, 1995b), Table 4.

**Table 5** Initial moles in the stripper gas-vapour phase (all units are kmol).

Substance	Base case	Mode 1	Mode 2	Mode 3
A	2.17937	2.36078	2.30908	2.22637
B	0.02237	0.02424	0.02370	0.02288
C	2.28017	2.46989	2.41458	2.33276
D	0.00584	0.00368	0.00014	0.00983
E	0.36552	0.27146	0.40736	0.06065
E	0.04458	0.09922	0.13894	0.03282
G	0.09894	0.11265	0.02145	0.16873
H	0.04070	0.05486	0.08688	0.00875

#### *Moles of each substance in the liquid*

The total moles in the liquid phase can be determined using the value of the moles of substance G,  $N_{G,\text{XII}}$  ((Ricker and Lee, 1995b), Table 4), along with the molar fraction of this compound at the stripping tower liquid outlet  $x_{G,11}$  ((Downs and Vogel, 1993), Table 1). This analysis is accurate since the authors specify that these moles of substance G are exclusively present in the liquid phase. The simple calculation is performed as follows:

$$N_{\text{XII}} = \frac{N_{G,\text{XII}}}{x_{G,11}} = \frac{21.74100}{0.53724} = 40.46795 \text{ kmol}.$$

The same result could be obtained by using the values for compound H. Next, to find the moles of each substance, the molar fraction of stream 11, as provided in the base case data ((Downs and Vogel, 1993), Table 1), is employed in the following way:

$$N_{i,\text{XII}} = x_{i,11} N_{\text{XII}}. \quad (35)$$

Finally, the results are reported in Table 6, with the observation that the values of G and H match those reported in (Ricker and Lee, 1995b), Table 4, whereas the remaining values are produced in the current work (not previously reported).

**Table 6** Initial moles in the stripper liquid phase (all units are kmol).

Substance	Base case	Mode 1	Mode 2	Mode 3
A	0.19384	0.19342	0.19762	0.14646
B	0.00364	0.00363	0.00371	0.00275
C	0.40792	0.40704	0.41586	0.30821
D	0.00728	0.00727	0.00743	0.00550
E	0.33831	0.33758	0.34490	0.25562
F	0.04006	0.03998	0.04084	0.03027
G	21.74100	21.74100	4.36330	38.99900
H	17.73629	17.73523	32.04743	3.53631

### *Partition coefficients $\phi_i$*

As mentioned previously, this coefficient enables the simplification of the typical gradient expression for mass transfer. Thus, the calculation is simply taking as mass transfer a fraction of the specific compound that enters the tower. Similar to the parameters of other equipment, these coefficients are determined from steady-state conditions. By utilizing the equations derived for the basic structure of the model ((23) and (24)) and setting the differential to zero, the following is obtained:

$$0 = y_{i,4} F_4 + \phi_i (x_{i,10} F_{10} + y_{i,4} F_4) - y_{i,5} F_5, \quad (36)$$

$$0 = x_{i,10} F_{10} - \phi_i (x_{i,10} F_{10} + y_{i,4} F_4) - x_{i,11} F_{11}, \quad (37)$$

where the only unknowns are the  $\phi_i$  values, as all the others are known parameters for the steady-state of the base case. Finally, the  $\phi_i$  values can be obtained from either (36) or (37).

## 5.4 Mixing point

This PS is straightforward as it comprises only a gas phase without reaction. The volume of the mixing point,  $V_{XIV} = 150 \text{ m}^3$ , can be directly extracted from Ricker and Lee (Ricker and Lee, 1995b). Likewise, the accumulation of moles of each compound in this equipment is fully documented in (Ricker and Lee, 1995b), Table 4.

## 6 Conclusions

In this paper, an exhaustive and complete dynamic model of the well-known Tennessee-Eastman (TE) process already reported in the literature has been presented. The proposed model has improved the mathematical description of some key parts of the

considered system while some other phenomena has been formalized and explained in a clearer way. The model, obtained by using a phenomenological-based semi-physical modelling (PBSM) approach well established in the literature, allows to simulate the behaviour of the entire system and its constitutive process systems for the four main modes of plant operation. Besides, it provides accurate information about the dynamical evolution of the variables and the suitable values of the constitutive parameters. All the equations and expressions for the computation of the system parameters are provided, fact that make the proposed model possible to be used for further tasks related to identification and the design of complex control strategies. Besides, the benchmark's versatility allows exploration of up to 15 reported faults in addition to the normal operation of the process. This feature enables users to apply and develop techniques for fault detection and diagnosis in a complex chemical process.

Future research directions opened by the proposed dynamic model include analyzing the computational efficiency of the numerical solution method and conducting a comprehensive assessment of the model's nonlinear behavior. This fact should incorporate key nonlinearity measures to determine whether generating linearized versions of the model would be appropriate or beneficial. This issue is a significant challenge due to the model's size (in terms of variables, parameters, and differential equations) and the stiff nature of the behaviours that it represents. Additionally, future research will also address the model's sensitivity to the chosen numerical integration method and explore the derivation of simplified dynamic models from the proposed formulation for use in estimation and automatic control applications. These simplified models, developed either through traditional model reduction methods or phenomenological simplification, are expected to outperform existing simpler models in their specific tasks.

**Acknowledgements.** This work was supported by the Agència de Gestió d'Ajuts Universitaris i de Recerca (AGAUR), Departament de Recerca i Universitats, Generalitat de Catalunya under Grant FI SDUR 2023 FISDU 00160, the Spanish project SEAMLESS: Sustainable learning-based Management of Multi-resource Largescale Systems (ref. PID2023-148840OB-I00), funded by MCIN/AEI/10.13039/501100011033/FEDER, UE, and the project "ACCIONES BILATERALES DE MOVILIDAD CONJUNTA CSIC 2025 MODALIDAD G, CSIC-UNAL-FACULTAD DE MINAS DE LA SEDE MEDELLÍN, COLOMBIA / BINAL25005".

## Declarations

- Funding. This work was supported in part by the Agència de Gestió d'Ajuts Universitaris i de Recerca (AGAUR), Departament de Recerca i Universitats, Generalitat de Catalunya and the Spanish project SEAMLESS: Sustainable learning-based Management of Multi-resource Large-scale Systems.
- Competing interests. All authors certify that they have no affiliations with or involvement in any organization or entity with any financial interest or non-financial interest in the subject matter or materials discussed in this manuscript.
- Code availability. The simulation code can be made available upon request.

- Author contribution. Conceptualization: [Mateo Arcila-Osorio], [Hernan Alvarez]; Project administration: [Mateo Arcila-Osorio], [Hernan Alvarez]; Methodology: [Mateo Arcila-Osorio], [Hernan Alvarez], [Carlos Ocampo-Martinez]; Funding acquisition: [Carlos Ocampo-Martinez]; Formal analysis: [Mateo Arcila-Osorio], [Hernan Alvarez]; Supervision: [Hernan Alvarez], [Carlos Ocampo-Martinez]; Validation: [Hernan Alvarez], [Carlos Ocampo-Martinez]; Resources: [Hernan Alvarez], [Carlos Ocampo-Martinez]; Writing - original draft: [Mateo Arcila-Osorio]; Writing - review & editing: [Mateo Arcila-Osorio], [Hernan Alvarez], [Carlos Ocampo-Martinez]. All authors read and approved the final manuscript.

## Appendix A Parameters values

In this appendix, the parameters values for the four basic modes of operation are reported. The table with the molar fractions of the compounds in the streams is not included for the base case, as this data was provided in full in the seminal article by [Downs and Vogel \(1993\)](#). However, the other determined parameters are displayed. Thus, Table [A1](#) corresponds to the base case, Tables [A2](#) and [A3](#) belong to mode 1, Tables [A4](#) and [A5](#) belong to mode 2, and Tables [A6](#) and [A7](#) correspond to mode 3.

**Table A1** Steady-state operating data (Base case).

Molar flow rates		Reactor		Flash separator	
stream	value (kmol/h)	reaction rates	value (kmol/h)	activity coefficients	value
$F_1$	11.200	$r_1$	114.246	$\gamma_D$	1.001779
$F_2$	114.500	$r_2$	92.943	$\gamma_E$	1.001389
$F_3$	98.000	$r_3$	0.012	$\gamma_F$	1.001247
$F_4$	417.500	reaction factors	value (kmol/h·m <sup>3</sup> )	$\gamma_G$	1.001584
$F_5$	465.700	$\alpha_1$	1.060311	$\gamma_H$	0.986491
$F_6$	1890.900	$\alpha_2$	1.021778	Stripping tower	
$F_7$	1476.100	$\alpha_3$	0.030827	partition coefficients	value
$F_8$	1201.500	activity coefficients	value	$\phi_A$	-0.004996
$F_9$	15.100	$\gamma_D$	0.994088	$\phi_B$	-0.009481
$F_{10}$	259.500	$\gamma_E$	0.995442	$\phi_C$	-0.010006
$F_{11}$	211.300	$\gamma_F$	0.995477	$\phi_D$	0.937722
$F_{15}$	1476.100	$\gamma_G$	0.998784	$\phi_E$	0.950208
$F_{17}$	1216.600	$\gamma_H$	0.994962	$\phi_F$	0.951603
		gas volume	value (m <sup>3</sup> )	$\phi_G$	0.074565
		$V_g$	20.24	$\phi_H$	0.039047

**Table A2** Molar fractions in the streams (Mode 1).

	Stream number					
	5 ( $y_{i,5}$ )	6 ( $y_{i,6}$ )	7 ( $y_{i,7}$ )	8 ( $y_{i,8}$ )	10 ( $x_{i,10}$ )	11 ( $x_{i,11}$ )
A	0.43744	0.32280	0.27936	0.32820	0.00000	0.00479
B	0.00449	0.14882	0.18488	0.21720	0.00000	0.00009
C	0.45766	0.18786	0.11185	0.13140	0.00000	0.01008
D	0.00068	0.06049	0.00770	0.00880	0.00138	0.00018
E	0.05030	0.16477	0.15010	0.15930	0.09750	0.00836
F	0.01838	0.04160	0.05220	0.05540	0.03392	0.00099
G	0.02087	0.04961	0.12911	0.06700	0.48439	0.53724
H	0.01017	0.02406	0.08480	0.03270	0.38281	0.43828

The molar fractions of streams 1, 2, 3, and 4 remain consistent with the base case (Downs and Vogel, 1993). Additionally, for each operation mode, it holds true that  $y_{i,15} = y_{i,7}$  and  $y_{i,17} = y_{i,9} = y_{i,8}$ .

**Table A3** Steady-state operating data (Mode 1).

Molar flow rates		Reactor		Flash separator	
stream	value (kmol/h)	reaction rates	value (kmol/h)	activity coefficients	value
$F_1$	11.991	$r_1$	113.932	$\gamma_D$	1.006460
$F_2$	114.314	$r_2$	92.737	$\gamma_E$	1.002289
$F_3$	96.471	$r_3$	0.725	$\gamma_F$	1.001987
$F_4$	413.782	reaction factors	value (kmol/h·m <sup>3</sup> )	$\gamma_G$	1.002796
$F_5$	456.460	$\alpha_1$	0.964985	$\gamma_H$	0.987094
$F_6$	2120.257	$\alpha_2$	1.024773	Stripping tower	
$F_7$	1704.081	$\alpha_3$	1.133081	partition coefficients	value
$F_8$	1441.021	activity coefficients	value	$\phi_A$	-0.005033
$F_9$	9.497	$\gamma_D$	0.997504	$\phi_B$	-0.009174
$F_{10}$	253.563	$\gamma_E$	0.993837	$\phi_C$	-0.010073
$F_{11}$	210.885	$\gamma_F$	0.993537	$\phi_D$	0.891184
$F_{15}$	1704.081	$\gamma_G$	0.996853	$\phi_E$	0.928690
$F_{17}$	1450.518	$\gamma_H$	0.997648	$\phi_F$	0.975725
		gas volume	value (m <sup>3</sup> )	$\phi_G$	0.077573
		$V_g$	22.08	$\phi_H$	0.047804

**Table A4** Molar fractions in the streams (Mode 2).

	Stream number					
	5 ( $y_{i,5}$ )	6 ( $y_{i,6}$ )	7 ( $y_{i,7}$ )	8 ( $y_{i,8}$ )	10 ( $x_{i,10}$ )	11 ( $x_{i,11}$ )
A	0.42744	0.34779	0.31309	0.36626	0.00000	0.00528
B	0.00439	0.08194	0.10060	0.11769	0.00000	0.00010
C	0.44697	0.19429	0.12505	0.14629	0.00000	0.01111
D	0.00003	0.01281	0.00114	0.00130	0.00020	0.00020
E	0.07541	0.25401	0.21168	0.22368	0.14105	0.00922
F	0.02572	0.05602	0.06974	0.07369	0.04647	0.00109
G	0.00397	0.00992	0.02582	0.01320	0.10012	0.11660
H	0.01608	0.04322	0.15288	0.05789	0.71215	0.85640

The molar fractions of streams 1, 2, 3, and 4 remain consistent with the base case (Downs and Vogel, 1993). Additionally, for each operation mode, it holds true that  $y_{i,15} = y_{i,7}$  and  $y_{i,17} = y_{i,9} = y_{i,8}$ .

**Table A5** Steady-state operating data (Mode 2).

Molar flow rates		Reactor		Flash separator	
stream	value (kmol/h)	reaction rates	value (kmol/h)	activity coefficients	value
$F_1$	13.848	$r_1$	22.908	$\gamma_D$	1.023592
$F_2$	22.948	$r_2$	167.624	$\gamma_E$	1.002491
$F_3$	174.679	$r_3$	1.386	$\gamma_F$	1.002505
$F_4$	383.109	reaction factors	value (kmol/h·m <sup>3</sup> )	$\gamma_G$	1.002206
$F_5$	432.296	$\alpha_1$	0.752475	$\gamma_H$	0.989306
$F_6$	2063.272	$\alpha_2$	1.029709	Stripping tower	
$F_7$	1679.49	$\alpha_3$	1.153484	partition coefficients	value
$F_8$	1419.501	activity coefficients	value	$\phi_A$	-0.005532
$F_9$	16.164	$\gamma_D$	1.014225	$\phi_B$	-0.010082
$F_{10}$	243.825	$\gamma_E$	0.994108	$\phi_C$	-0.011071
$F_{11}$	194.638	$\gamma_F$	0.994107	$\phi_D$	0.223904
$F_{15}$	1679.49	$\gamma_G$	0.993942	$\phi_E$	0.947839
$F_{17}$	1435.665	$\gamma_H$	0.994214	$\phi_F$	0.981251
		gas volume	value (m <sup>3</sup> )	$\phi_G$	0.070330
		$V_g$	22.08	$\phi_H$	0.040041

**Table A6** Molar fractions in the streams (Mode 3).

	Stream number					
	5 ( $y_{i,5}$ )	6 ( $y_{i,6}$ )	7 ( $y_{i,7}$ )	8 ( $y_{i,8}$ )	10 ( $x_{i,10}$ )	11 ( $x_{i,11}$ )
A	0.45784	0.29466	0.22754	0.27860	0.00000	0.00338
B	0.00471	0.27788	0.36819	0.45080	0.00000	0.00006
C	0.47972	0.17966	0.07530	0.09220	0.00000	0.00712
D	0.00202	0.12675	0.01852	0.02180	0.00389	0.00013
E	0.01247	0.03849	0.03742	0.03940	0.02859	0.00591
F	0.00675	0.01293	0.01729	0.01820	0.01322	0.00070
G	0.03470	0.06615	0.23754	0.09400	0.87727	0.90100
H	0.00180	0.00349	0.01820	0.00500	0.07703	0.08170

The molar fractions of streams 1, 2, 3, and 4 remain consistent with the base case (Downs and Vogel, 1993). Additionally, for each operation mode, it holds true that  $y_{i,15} = y_{i,7}$  and  $y_{i,17} = y_{i,9} = y_{i,8}$ .

**Table A7** Steady-state operating data (Mode 3).

Molar flow rates		Reactor		Flash separator	
stream	value (kmol/h)	reaction rates	value (kmol/h)	activity coefficients	value
$F_1$	8.703	$r_1$	161.664	$\gamma_D$	1.000023
$F_2$	161.856	$r_2$	14.645	$\gamma_E$	0.999591
$F_3$	15.216	$r_3$	0.195	$\gamma_F$	0.998581
$F_4$	350.844	reaction factors	value (kmol/h·m <sup>3</sup> )	$\gamma_G$	1.000310
$F_5$	370.335	$\alpha_1$	1.052162	$\gamma_H$	0.985923
$F_6$	1436.940	$\alpha_2$	1.023548	Stripping tower	
$F_7$	1083.237	$\alpha_3$	1.315352	partition coefficients	value
$F_8$	880.830	activity coefficients	value	$\phi_A$	-0.003560
$F_9$	3.895	$\gamma_D$	0.995826	$\phi_B$	-0.006488
$F_{10}$	198.512	$\gamma_E$	0.995854	$\phi_C$	-0.007124
$F_{11}$	179.021	$\gamma_F$	0.995019	$\phi_D$	0.970502
$F_{15}$	1083.237	$\gamma_G$	0.998715	$\phi_E$	0.813732
$F_{17}$	884.725	$\gamma_H$	0.999190	$\phi_F$	0.952296
		gas volume	value (m <sup>3</sup> )	$\phi_G$	0.073787
		$V_g$	22.08	$\phi_H$	0.043565



## References

- Andersen, E., A. Udugama, I., Gernaey, K., Khan, A., Bayer, C., Kulahci, M.: An easy to use GUI for simulating big data using Tennessee Eastman process. *Quality and Reliability Engineering International* **38** (2021) <https://doi.org/10.1002/qre.2975>
- Arbeláez-Gómez, D., Benavides-López, S., Giraldo-Agudelo, M.P., Guzmán-Álvarez, J.P., Ramírez-Mazo, C., Gómez-Echavarría, L.M.: A phenomenological-based model of the endometrial growth and shedding during the menstrual cycle. *Journal of Theoretical Biology* **532**, 110922 (2022) <https://doi.org/10.1016/j.jtbi.2021.110922>
- Alvarez, H.: Phenomenological-based semi-physical models, formalizing the tool. In: Chakraborty, S., Curcio, S. (eds.) *Advanced Modelling and Simulation in the Chemical and Biochemical Process Industry*, pp. 43–71. CRC Press, Boca Raton, Florida, EEUU (2024)
- Alvarez, H., Lamanna, R., Vega, P., Revollar, S.: Metodología para la obtención de modelos semifísicos de base fenomenológica aplicada a una sulfitadora de jugo de caña de azúcar. *Revista Iberoamericana de Automática e Informática Industrial RIAI* **6**(3), 10–20 (2009) [https://doi.org/10.1016/S1697-7912\(09\)70260-2](https://doi.org/10.1016/S1697-7912(09)70260-2)
- Alvarez, H., Ocampo-Martinez, C.: A phenomenological-based dynamic model for a polymer electrolyte membrane fuel-cell humidifier assembly. *Journal of Power Sources* **547**, 231985 (2022) <https://doi.org/10.1016/j.jpowsour.2022.231985>
- Budman, H.M., Douglas, P.L., Ricardez-Sandoval, L.A.: Simultaneous Design and Control of the Tennessee Eastman Process. *IFAC Proceedings Volumes* **41**(2), 12911–12916 (2008) <https://doi.org/10.3182/20080706-5-KR-1001.02183> . 17th IFAC World Congress
- Bathelt, A., Ricker, N.L., Jelali, M.: Revision of the Tennessee Eastman Process Model. *IFAC-PapersOnLine* **48**(8), 309–314 (2015) <https://doi.org/10.1016/j.ifacol.2015.08.199> . 9th IFAC Symposium on Advanced Control of Chemical Processes ADCHEM 2015
- Chadha, G.S., Schwung, A.: Comparison of deep neural network architectures for fault detection in Tennessee Eastman process, 1–8 (2017) <https://doi.org/10.1109/ETFA.2017.8247619>
- Downs, J.J., Vogel, E.F.: A plant-wide industrial process control problem. *Computers & Chemical Engineering* **17**(3), 245–255 (1993)
- Elorza Casas, C.A., Valipour, M., Ricardez Sandoval, L.A.: Multi-scenario and multi-stage robust NMPC with state estimation application on the Tennessee-Eastman process. *Control Engineering Practice* **139**, 105635 (2023) <https://doi.org/10.1016/j.conengprac.2023.105635>

- Hangos, K., Cameron, I.T.: Process Modelling and Model Analysis vol. 4, p. 543. Academic Press, United States of America (2001)
- Hartung, F., Franks, B.J., Michels, T., Wagner, D., Liznerski, P., Reithermann, S., Fellenz, S., Jirasek, F., Rudolph, M., Neider, D., Leitte, H., Song, C., Kloepper, B., Mandt, S., Bortz, M., Burger, J., Hasse, H., Kloft, M.: Deep Anomaly Detection on Tennessee Eastman Process Data. *Chemie Ingenieur Technik* **95**(7), 1077–1082 (2023) <https://doi.org/10.1002/cite.202200238> <https://onlinelibrary.wiley.com/doi/pdf/10.1002/cite.202200238>
- Jämsä, N.: Model predictive control for the Tennessee Eastman process. Master’s thesis, Aalto University, School of chemical engineering (January 2018). Available at <https://urn.fi/URN:NBN:fi:aalto-201804031968>
- Jockenhövel, T., Biegler, L.T., Wächter, A.: Dynamic optimization of the Tennessee Eastman process using the OptContolCenter. *Computers & Chemical Engineering* **27**(10), 1513–1531 (2003)
- Kano, M., Nagao, K., Hasebe, S., Hashimoto, I., Ohno, H., Strauss, R., Bakshi, B.R.: Comparison of multivariate statistical process monitoring methods with applications to the Eastman challenge problem. *Computers & Chemical Engineering* **26**(2), 161–174 (2002) [https://doi.org/10.1016/S0098-1354\(01\)00738-4](https://doi.org/10.1016/S0098-1354(01)00738-4)
- Lawrence Ricker, N.: Decentralized control of the Tennessee Eastman Challenge Process. *Journal of Process Control* **6**(4), 205–221 (1996) [https://doi.org/10.1016/0959-1524\(96\)00031-5](https://doi.org/10.1016/0959-1524(96)00031-5)
- Lema-Perez, L., Garcia-Tirado, J., Builes-Montaño, C., Alvarez, H.: Phenomenological-based model of human stomach and its role in glucose metabolism. *Journal of Theoretical Biology* **460**, 88–100 (2019)
- Lema-Perez, L., Muñoz-Tamayo, R., Garcia-Tirado, J., Alvarez, H.: On parameter interpretability of phenomenological-based semiphysical models in biology. *Informatics in Medicine Unlocked* **15**, 100158 (2019) <https://doi.org/10.1016/j.imu.2019.02.002>
- Martin-Villalba, C., Urquia, A., Shao, G.: Implementations of the Tennessee Eastman Process in Modelica. *IFAC-PapersOnLine* **51**(2), 619–624 (2018) <https://doi.org/10.1016/j.ifacol.2018.03.105> . 9th Vienna International Conference on Mathematical Modelling
- Ravi Srinivas, G., Arkun, Y.: Control of the Tennessee Eastman process using input-output models. *Journal of Process Control* **7**(5), 387–400 (1997) [https://doi.org/10.1016/S0959-1524\(97\)00015-2](https://doi.org/10.1016/S0959-1524(97)00015-2) . *Nonlinear Process Control*
- Reinartz, C., Enevoldsen, T.T.: pyTEP: A Python package for interactive simulations of the Tennessee Eastman process. *SoftwareX* **18**, 101053 (2022) <https://doi.org/>

[10.1016/j.softx.2022.101053](https://doi.org/10.1016/j.softx.2022.101053)

- Ricker, N.L.: Model predictive control of a continuous, nonlinear, two-phase reactor. *Journal of Process Control* **3**(2), 109–123 (1993) [https://doi.org/10.1016/0959-1524\(93\)80006-W](https://doi.org/10.1016/0959-1524(93)80006-W)
- Ricker, N.L., Lee, J.H.: Nonlinear model predictive control of the tennessee eastman challenge process. *Computers & Chemical Engineering* **19**(9), 961–981 (1995) [https://doi.org/10.1016/0098-1354\(94\)00105-W](https://doi.org/10.1016/0098-1354(94)00105-W)
- Ricker, N.L., Lee, J.H.: Nonlinear modeling and state estimation for the Tennessee Eastman challenge process. *Computers & Chemical Engineering* **19**(9), 983–1005 (1995)
- Tătulea-Codrean, A., Fischer, J., Engell, S.: A Multi-stage Economic NMPC for the Tennessee Eastman Challenge Process. *IFAC-PapersOnLine* **53**(2), 6069–6075 (2020) <https://doi.org/10.1016/j.ifacol.2020.12.1678> . 21st IFAC World Congress
- Tian, Z., Hoo, K.A.: Transition control using a state-shared model approach. *Computers & Chemical Engineering* **27**(11), 1641–1656 (2003) [https://doi.org/10.1016/S0098-1354\(03\)00131-5](https://doi.org/10.1016/S0098-1354(03)00131-5)
- Udugama, I.A., Gernaey, K.V., Taube, M.A., Bayer, C.: A novel use for an old problem: The Tennessee Eastman challenge process as an activating teaching tool. *Education for Chemical Engineers* **30**, 20–31 (2020) <https://doi.org/10.1016/j.ece.2019.09.002>
- Vosloo, J., Uren, K.R., van Schoor, G.: A complete and open Simulink model of the Tennessee Eastman process (COSTEP). *SoftwareX* **31**, 102217 (2025) <https://doi.org/10.1016/j.softx.2025.102217>
- Zerkaoui, S., Druaux, F., Leclercq, E., Lefebvre, D.: Indirect neural control for plant-wide systems: Application to the Tennessee Eastman Challenge process. *Computers & Chemical Engineering* **34**(2), 232–243 (2010) <https://doi.org/10.1016/j.compchemeng.2009.08.003>
- Zhou, J., Zhu, Y.: Fault isolation based on transfer-function models using an MPC algorithm. *Computers & Chemical Engineering* **159**, 107668 (2022) <https://doi.org/10.1016/j.compchemeng.2022.107668>